Resistance Driven H_2 Gas Sensor: High Entropy Alloy Nanoparticles Decorated 2D MoS_2

Bidesh Mondal[1], Xiaolei Zhang[2], Sumit Kumar[3], Feng Long[2,4], Nirmal Kumar Katiyar[5], Mahesh Kumar[3], Saurav Goel*[5,6] and Krishanu Biswas[1]**

[1] *Department of Materials Science and Engineering, Indian Institute of Technology Kanpur, Kanpur, India, 208016*

[2] *Department of Chemical and Process Engineering, University of Strathclyde, Glasgow, UK*

[3] *Department of Electrical Engineering, Indian Institute of Technology Jodhpur, India*

[4]*Institute of Chemical Industry of Forest Products, Chinese Academy of Forestry, Nanjing 210042, China*

[5]*School of Engineering, London South Bank University, London UK, SE1 0AA*

[6]*University of Petroleum and Energy Studies, Dehradun 248007, India*

Krishanu Biswas, *Department of Materials Science and Engineering, Indian Institute of Technology Kanpur, Kanpur, India, 208016*

Email: kbiswas@iitk.ac.in

Mahesh Kumar*, Department of Electrical Engineering, Indian Institute of Technology Jodhpur, India*

Email: mkumar@iitj.ac.in

Saurav Goel *School of Engineering, London South Bank University, London UK, SE1 0AA;*

Email: goels@lsbu.ac.uk

Abstract

The need for using Hydrogen (H_2) gas has increasingly become important due to the growing demand for carbon-free energy sources. However, the explosive nature of H_2 gas possess significant safety concerns, driving the development of efficient and reliable detection. Although 2D materials have emerged as promising for hydrogen gas sensing applications due to their relatively high sensitivity; the incorporation of other nanomaterials into 2D materials can drastically improve both the selectivity and sensitivity of sensors. In this work, the high entropy alloy nanoparticles using non-noble metals were used to develop a sensor for H_2 gas detection. This chemical sensor was realized by decorating the 2D MoS_2 surfaces with multicomponent body-centered cubic (BCC) equiatomic Ti-Zr-V-Nb-Hf high entropy alloy (HEA) nanoparticles. It was selective towards H_2, compared to NH_3, H_2S, CH_4, and C_4H_{10}, demonstrating widespread applications of this sensor. To understand the mechanisms behind abnormal selectivity and sensitivity, density functional theory (DFT) calculations were performed, showing that the HEA nanoparticles can act as a chemical hub for H_2 adsorption and dissociation, ultimately improving the performance of 2D material-based gas sensors.

Keywords: Gas sensor, High entropy alloys, 2D MoS_2, H_2 sensors, DFT

Introduction

Hydrogen (H_2) gas has been emerging as a global focus of attention due to being a green source of energy and it is envisioned that the switch to a Hydrogen economy will eliminate our excessive reliance on fossil fuels; [1] a vital move towards a carbon-neutral economy. H_2 is a zero-carbon feedstock that is abundant, odorless, highly flammable and has high energy per mass but it is explosive and highly imflammable.[2] Therefore, the frequent and widespread use of hydrogen gas is associated with fire and explosion hazards that can be overcome by efficient sensors having high selectivity and high specificity, as preventive measures of a major accident at critical sites such as industrial workplaces, transportation, hospitals, airports, laboratories, etc.

Various sensors for hydrogen gas sensing have been reported in literature. Pd metal as a nanomaterial works well for sensing because it can dissociate H_2 molecules and possess high absorption affinity towards H_2[3]. Pd experiences volumetric expansion upon reaction with H_2, enabling it to achieve resistance-driven sensing[4]. However, increasing the temperature reduces the sensing performance of Pd due to the reduction of solubility of H_2 in Pd through the formation of PdH_x.[5] It has been found that coating the Pd metal nanowires with Pt metal doubles the performance of H_2 detection in terms of sensitivity and recovery time.[6] Other studies have shown that the addition of Au and Cu in the Pd metal (Ternary alloy) enhances the response and recovery for H_2 gas sensing. The supporting element Cu reduces the CO poisoning and deactivation, and Au metal reduces the hydrogen sorption apparent activation energy and provides enhanced response and recovery.[7, 8]

H_2 sensing often use precious metals which can be offset by use of low-cost materials for detection of H_2 gas. The high-entropy alloy (HEA) nanoparticles have exceptional properties which can be tuned for a specific purpose[9] The decoration of high entropy alloy nanoparticles (AgAuCuPdPt) on 2D MoS_2, where Pd metal was diluted in a 2:10 ratio along with other supporting elements (Pt, Au) showed enhanced H_2 selectivity as well as response gain from 2% to 30%.[10] However, this type of sensor material is too expensive for any technological application and hence, the need to develop HEA nanoparticles to devoid the expensive Pt group metals became the primary motivation of this work.

HEAs can further be tuned to develop a materials system that can offer high selectivity and sensitivity for H_2 adsorption based on a resistance-driven sensor. Accordingly, the research entails the decoration of MoS_2 2D sheets with relatively cheaper body-centered cubic (BCC) high entropy alloy nanoparticles (equiatomic Ti-Zr-V-Nb-Hf). The presence of these HEA nanoparticles over

the MoS_2 surface was observed to facilitate H_2 adsorption, enhancing the sensing response seven times. We intend to investigate and clarify the underlying H_2 adsorption and resistance variation mechanism using Density Functional Theory (DFT). The work compares and benchmarks the performance of two candidate materials tested here namely, 2D MoS_2 and Ti-Zr-V-Nb-Hf HEA nanoparticles (NPs) decorated 2D MoS_2, which were designated as bare MoS_2 and HEA: MoS_2 for ease of description.

Materials and Methods

HEAs nanoparticles preparation

The Ti, Zr, V, Nb, and Hf metals with 99.99% assay were purchased from Theromfisher scientific® in the form of chips/buttons. In equimolar ratio, all metals were melted in the Arc melting furnace under an Ar environment to avoid the oxidation of metals to form a metal ingot. The ingot comprising all five elements was melted multiple times to ensure chemical homogeneity. Thus, the ingot was homogenized at 1473 K in a vacuum-sealed quartz tube for 10 hours and quenched in cold water to freeze the high-temperature single phase. Afterward, the ingot was parted into smaller pieces and milled at extremely low temperatures (<123 K) using a custom-built cryomill for 6 h.[11-13] The whole process is known as casting-cum-comminution method and it is very useful to prepare nanocrystalline high entropy alloys.[14, 15] The materials selection and methodology followed can be seen from the supporting information shown in Fig.S1. The alloy composition selected in this work was predicted by the ThermoCalc software to reside in the BCC phase and the relevant equilibrium phase diagram is shown in the supporting information in Fig. S2.

Decoration of HEAs NPs on MoS_2

The cryomilled HEA nanoparticles were dispersed in ultrapure methanol. The MoS_2 sheets were also cryomilled for 6 h to form MoS_2 nanosheets, and then the sheets were dispersed in Dimethyl sulfoxide (DMSO) solvent and ultrasonicated for 30 hours for their exfoliation using a 1500 W ultrasonicator. During ultrasonication, 0.1 wt% HEA NPs was added into exfoliated MoS_2 for their decoration and ultrasonicated for 10 hours.

Sensing device fabrication and characterization

The drop-casting method was used to fabricate the sensor device. The SEM image of the gas sensor is shown in Fig 2a. The Au (200 nm)/Cr (30 nm) interdigitated electrode (IDE) patterns were fabricated on SiO_2/Si substrate by using the thermal evaporation technique. The distance between the interdigitated electrodes was 200 µm. The sensor was obtained by dropping MoS_2 and MoS_2: HEA dispersion on SiO_2/Si substrate with a 5 µl droplet of 5 mg/1 ml solution of MoS_2 and HEA (2.5 mg): MoS_2 (2.5 mg) of prepared suspension. The gas sensing was shown by the measurement of the resistance change with target gases. The resistance signal was recorded under a direct biasing voltage of 2V by using a Keithly Source meter (2636B). In the testing measurement system for the resistance-type gas sensor, the biasing voltage was directly applied to an electrode. The initial current value stabilized in ambient air and when the target gas is introduced into the chamber the current signals rapidly increase, which can be easily measured by using a source meter. The sensor response can be defined as:

$$Response\ (\%) = \frac{\Delta R}{R_a} = \frac{(R_a - R_g)}{R_a} \times 100\ \%$$

where R_a and R_g reveal resistance value of the sensor in the background gas and H_2/NO_2 or other test gases, respectively.

Characterisation

DFT modelling

All the structural optimisation and electronic calculations were obtained adopting density functional theory (DFT) using the Vienna Ab Initio Simulation Package (VASP).[16, 17] The DFT exchange-correlation contribution was calculated using Generalized Gradient Approximation (GGA) through Perdew-Burke-Ernzerhof (PBE) functional. The Grimme method was used for DFT dispersion correction.[18] The self-consistent calculation and optimisation with the convergence criteria $=1\times10^{-4}$ eV, and the convergence threshold for forces <0.05 eV. The cut-off energy was set at a fine level with 450 eV and the K-point was set as 3×3×1. During the structural optimisation, the bottom layer was fixed and the top two layers were allowed to relax. The density of states (DOS) was analysed with an energy range of 10 eV and a fine level of K-point set. The DOS was analysed for each structure to distinguish contributions according to the angular momentum of the states. The adsorption energies (E_{ads}) were calculated using the equation:

$$E_{ads} = E(Catalyst) + E(H_2) - E(H_2/Catalyst)$$

where E(Catalyst), E(H_2) and E(H_2/Catalyst) are respective energies of catalysts (including MoS_2 and HEA/MoS_2), H_2 and H_2 absorbed on the catalysts.

Results and discussions

Materials characteristics

To comprehend the sensing properties, it is necessary to grasp the characteristics of the material. The material synthesis of equiatomic HEA (Ti-Zr-V-Nb-Hf) was performed using vacuum arc melting, which produced the bulk HEA by melting the metallic elements in the required proportions. The HEA nanoparticles were produced by cryomilling of bulk HEA at an extremely low temperature, providing fully nanocrystalline BCC phase HEA (Ti-Zr-V-Nb-Hf)

nanoparticles.[19] Under the ThermoCalc predictions, the bulk HEA and HEA NPs both showed single-phase BCC structure by X-ray diffraction, as shown in Fig. 1a. The broadening of the diffraction peaks after cryomilling indicated the formation of nanocrystalline material. The size of HEA NPs was about 12 ± 5 nm; which was measured using bright field transmission electron microscopy (TEM), as depicted in Fig. 1(b-d), the the corresponding distribution of size can be seen from the histogram shown in Supporting information Fig. S5. Cryomilling was also used to transform bulk MoS_2 into nanosheets, which were subsequently exfoliated into 2D layers via ultrasonication for a long duration (20 h). The formation of 2D layers was confirmed by a TEM bright field micrograph illustrated in Fig.1e. As the ultrasonication process unfolded, NPs of HEA were introduced to the 2D-MoS_2 sheets, entrapped either between the 2D sheets or atop the 2D MoS_2 surface. A bright field TEM micrograph, as depicted in Fig.1g confirmed the presence of nanoparticles over the 2D-MoS_2 layer. The AFM image in Fig.1h confirmed anchoring of NPs with a height of about 10-12 nm (typical size of HEA NP) over the MoS_2 nanosheets. When nanoparticles were added to the surface of 2D MoS_2, the resulting Raman spectrum showed a shift of 5 cm^{-1} Raman band with a slight increase in the peak intensity.

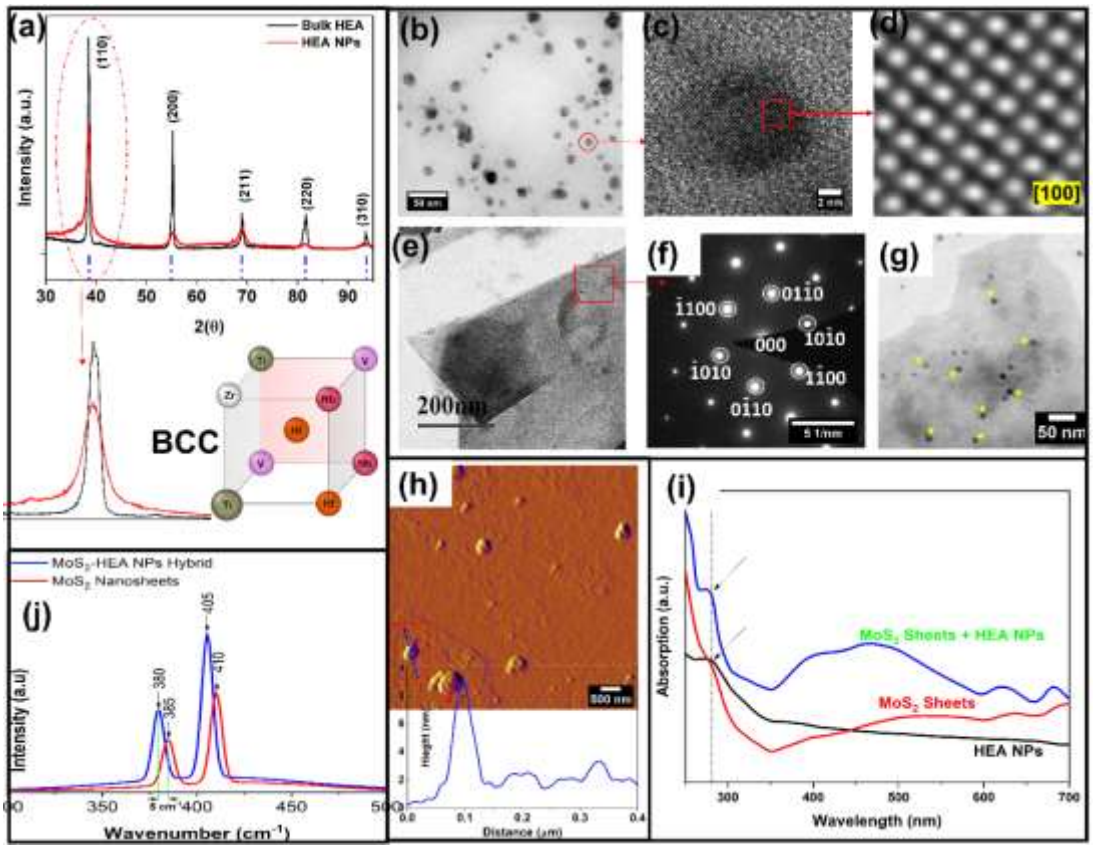

Fig.1 Materials characterization **(a)** X-ray diffraction pattern of HEA bulk and NPs, **(b)** bright filed TEM micrograph of nanoparticles, **(c)** HRTEM of Ti-Zr-V-Nb-Hf nanoparticles, **(d)** FFT Filtered HRTEM **(e)** bright field TEM micrograph of exfoliated MoS_2, **(f)** selected area diffraction pattern exfoliated MoS_2, **(g)** bright field TEM micrograph Ti-Zr-V-Nb-Hf nanoparticles decorated over MoS_2 sheet **(h)** AFM micrograph of NPs decorated over MoS_2, inset shows the height profile of NPs**, (i)** SPR response of NPs in MoS_2, **(j)** Raman shift of 2D MoS_2 sheet and decorated MoS_2 with NPs,

The Raman shift can be attributed to charge redistribution and the local surface plasmon resonance of the high-entropy alloy (HEA) nanoparticles [20-22] (Fig. 1j). Additionally, a surface plasmon band was observed at 270 nm for the HEA nanoparticles, both with and without decoration on MoS_2 (Fig.1i). [10]

I-V Characteristics Sensors

The current-voltage (I-V) behavioour of bare MoS_2 and HEA nanoparticles decorated MoS_2 sensors are shown in Fig. 2a and 2b. From Fig. 2a it can be inferred that the sensor showed a linear I-V characteristic consistent with the expected behaviour of bare MoS_2.[23] However, the

heterojunction of metal NPs and semiconductors exhibited a non-linear I-V relationship identical to theSchottky nature.[24-26] This behavior was accompanied by a significant increase in the conductance of the device . This phenomenon may be attributed to a modification in the potential of the MoS_2 composite in presence of HEA NPs. Nevertheless, both devices exhibited a semiconducting nature, specifically, a decrease in resistance on heating.[27]

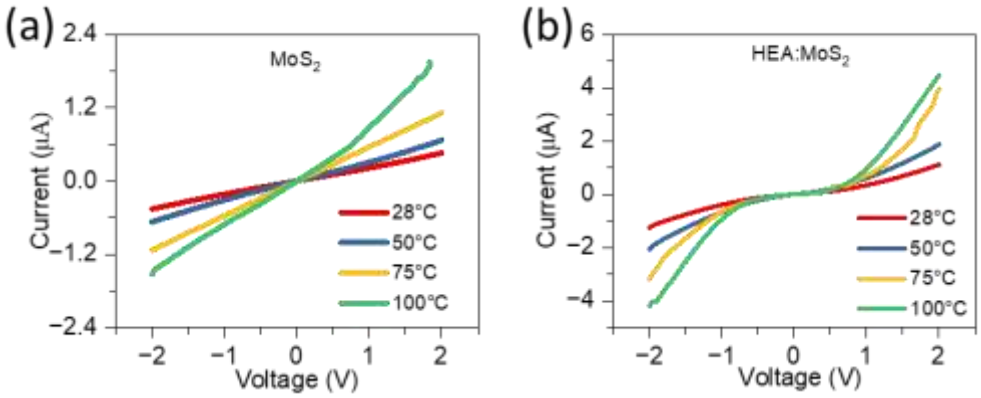

Fig. 2 (a) schematic of the sensor device, (b) current–voltage (I–V) characteristics of devices fabricated using bare MoS_2 and (c) HEA: MoS_2 composite as a function of temperature, (d) comparison of the linearity and current of both devices at 28 °C.

Sensor Characteristics

The sensor device was assembled and tested under controlled conditions using various gases (H_2, H_2S, NH_3, CH_4, and C_4H_{10}). The dynamic resistive response of the IDE pattern, both with and without HEA NPs decoration over 2D MoS_2 sheets was recorded at various temperature and concentration of targeted gases over time. At room temperature, the 2D MoS_2 sheet exhibited a relative resistance response of 10%, which vary slightly with the increase of temperature (see Fig.3b).

On the other hand, the response of HEA:2D MoS_2 showed a sudden increase in current resulting in a 47% relative resistance response, and it maintained the dynamic response up to an operating temperature of 75°C. However, the sensing response decreases when the operating temperature is raised to 100°C, as shown in Fig. 3(c-d). Despite this decrease in sensing response, the sensor remained highly selective towards H_2 gas and did not show a significant response towards other gases such as NH_3, H_2S, CH_4, and C_4H_{10} both with and without HEA NPs decoration over MoS_2, as demonstrated in Fig. 3(e-f). When operated at 50°C, the HEA: MoS_2 sensor showed a response of 20% at 1 ppm H_2, which increased to 47% as the concentration of H_2 gas increased to 50 ppm.

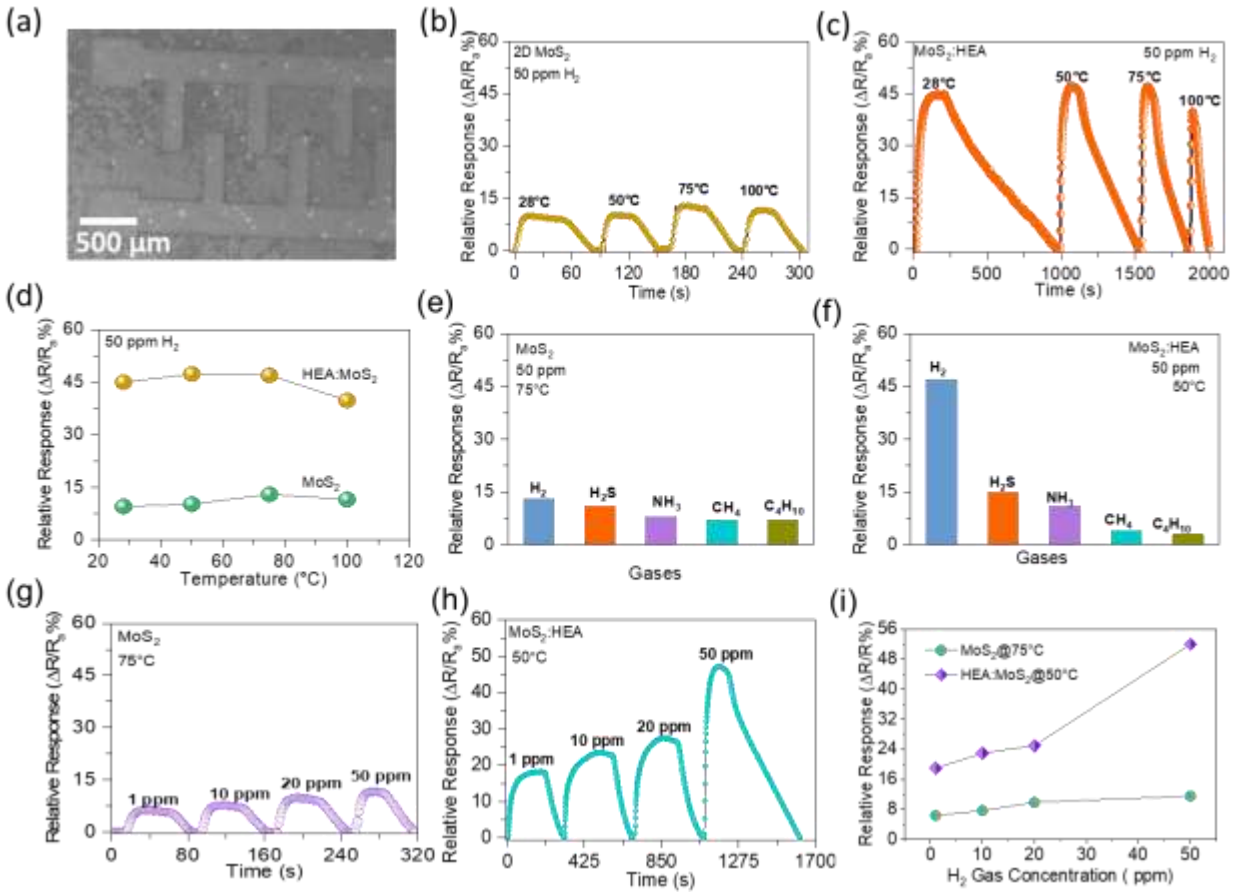

Fig. 3 (a) SEM image of the sensor with interdigitated electrodes (IDE) pattern, **(b)** relative response of 2D MoS_2, **(c)** relative response of MoS_2 embedded with HEA nanoparticles against time and temperature, **(d)** comparison of the response of 2D MoS_2 vs 2D MoS_2+HEA NPs, **(e)**

selectivity of different gases on 2D MoS_2, **(f)** selectivity of different gases on MoS_2 + HEA NPs, **(g)** relative response of MoS_2 against time and H_2 gas concentration, **(h)** relative response of 2D MoS_2 embedded with HEA nanoparticles against time and H_2 concentration, **(i)** cooperative response of both bare and nanocomposite based.

In contrast, the bare MoS_2 sensor only showed a response of 7%, which was limited to a maximum of 12%, as depicted in Fig. 3(g-h).

Learnings from the DFT simulations

To understand the gas sensing mechanism, it is essential to evaluate the adsorption energy of targeted molecules on the sensing surface.[28, 29] The DFT calculations were carried out to investigate the influence of adding HEA clusters on 2D MoS_2 sheets which was seen to enhance the H_2 adsorption. The DFT models constructed two catalyst systems for the adsorption of H_2: pristine MoS_2 and the HEA NPs doped MoS_2. These are subsequently named H_2-MoS_2 and H_2-HEA-MoS_2 respectively. The results showed that the adsorption energy of H_2 on MoS_2 was 0.06 eV on site-1 and 0.66 eV on site-2 (sites marked in Fig. 4a and their corresponding adsorption energy are shown in Table 1). The adsorption energy of H_2 on the HEA-MoS_2 surface was observed to increase significantly in most cases, ranging from 0.07 to 5.75 eV depending on the location of adsorption site. Interestingly, it was found that the adsorption energy on top of the HEA sites was lower than the energy of site-2 of pure MoS_2, and the adsorption energy on the H_2-HEA-MoS_2 system increased beyond 5 eV when H_2 was adsorbed on the interface between the HEA cluster and MoS_2 surface. Furthermore, the adsorption energies dramatically increased when H_2 was adsorbed on sites 8-20 and exhibited the largest adsorption energies on sites 21-24. Site 21 revealed an adsorption energy of 4.36 eV due to the presence of the *Zr* atom connected with the Mo and S atoms, and sites 22-24 had large adsorption energies ranging from 4 to 5.75 eV due to the HEA cluster promoting the adsorption performance of the Mo atoms. Additionally, the H_2 had

strong adsorption of 5.50 eV but it dissociates and gets adsorbed on 21-9 and 21-6 bridge sites. A schematic concerning this is shown in Fig. 4b, to highlight the influence of nanoparticles at the NPs-MoS_2 interface, which facilitated more H_2 adsorption and dissociation to enhance the sensing signal. Overall, the study suggests that loading HEA clusters on the MoS_2 surface improves H_2 adsorption capability by virtue of electronic charge redistribution of NPs over the support materials.[30]

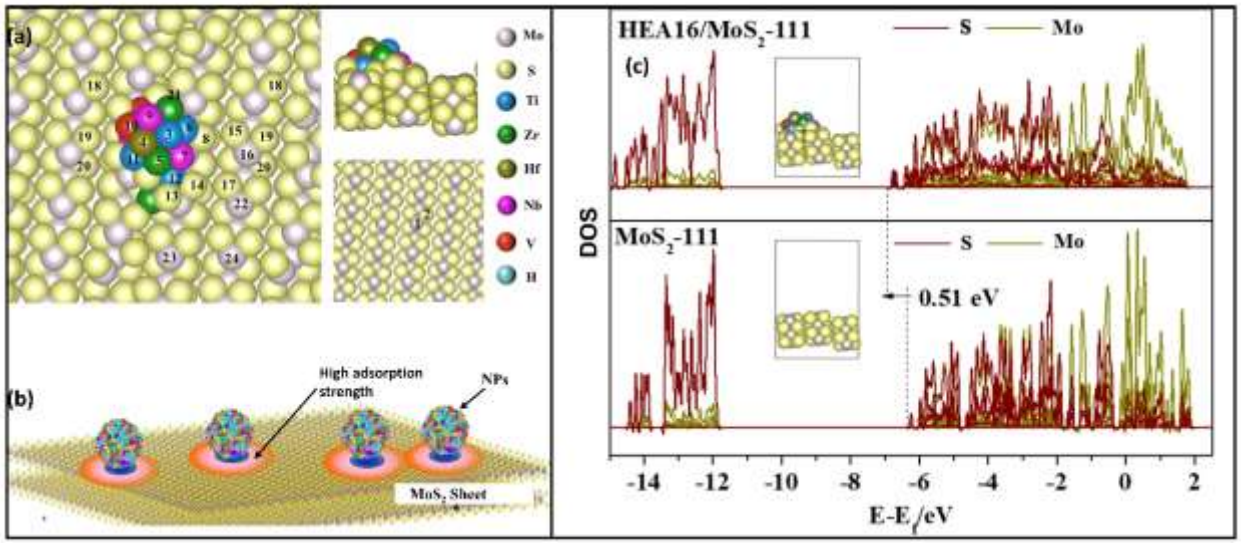

Fig. 4 (a) Adsorption sites of the H_2 adsorbed on the MoS_2 and HEA-MoS_2 catalyst system; marked number position corresponding adsorption energy in Table 1, **(b)** A schematics of HEA NPs and MoS_2 interface influences, **(c)** DOS of the MoS_2 on the MoS_2 and HEA-MoS_2 system.

Table 1. H_2 adsorption energies of the H_2 absorbed on the different sites.

Site	E_{ads}	Site	E_{ads}	Site	E_{ads}
1	0.66	9	3.69	17	3.26
2	0.07	10	3.76	18	3.29
3	0.07	11	3.46	19	3.29
4	0.20	12	3.57	20	3.27
5	0.32	13	3.27	21	4.36
6	0.37	14	3.28	22	4.11
7	0.42	15	3.27	23	5.75
8	3.46	16	3.26	24	4.03

Furthermore, the bandgap and density of states (DOS) of MoS_2 were also examined in both MoS_2 and HEA-MoS_2 systems. It was seen that the bandgap of MoS_2 reduces from 0.11 eV to 0.05 eV while the MoS_2 is decorated by the HEA cluster. The DOS of the MoS_2 in the HEA-MoS_2 system was observed to shift down to the Fermi level at around 0.51 eV compared to the MoS_2 system, as demonstrated in Fig. 4c. The shifting Fermi level makes electron transfer from H_2 molecules more favourable to the HEA: MoS_2 system. [31] However, the influence of NP is limited to the surroundings to adsorb and dissociate the H_2 molecules, and the high adsorption energy at the MoS_2-NPs interface is directly responsible for the increased sensor response. These findings suggest that the HEA nanoparticle interface plays a crucial role in facilitating interactions that enhance the sensor response against selective gases, especially hydrogen.

Gas sensing mechanism

The electronic properties of a 2D MoS_2 sheet are influenced by various factors such as doping and environmental conditions. In its pure state, 2D MoS_2 is an intrinsic semiconductor with a direct bandgap, allowing for both electron and hole conduction.[32] However, decorating MoS_2 with high

entropy alloy (HEA) nanoparticles, which consist of Ti, Zr, V, Nb, and Hf, polarizes the material and influences the overall bandgap. The decorated MoS_2 possess n-type semiconductor behaviour which can be seen through the I-V characteristics and the shift of Raman peak demonstrated the charge redistribution. Charge transfer from NP to MoS_2 induces n-type behavior and enhances the interface's reactivity towards H_2 molecules' adsorption.[30] As a reducing gas, hydrogen molecules transfer electrons to the HEA: MoS_2 interface, which is further facilitated by the downward shift of the Fermi level, as predicted by the DFT calculations. Adsorbed hydrogen molecules undergo dissociation to provide electrons to the sample, resulting in an increased electric current. A schematic representation of this process is shown in Fig. 5.

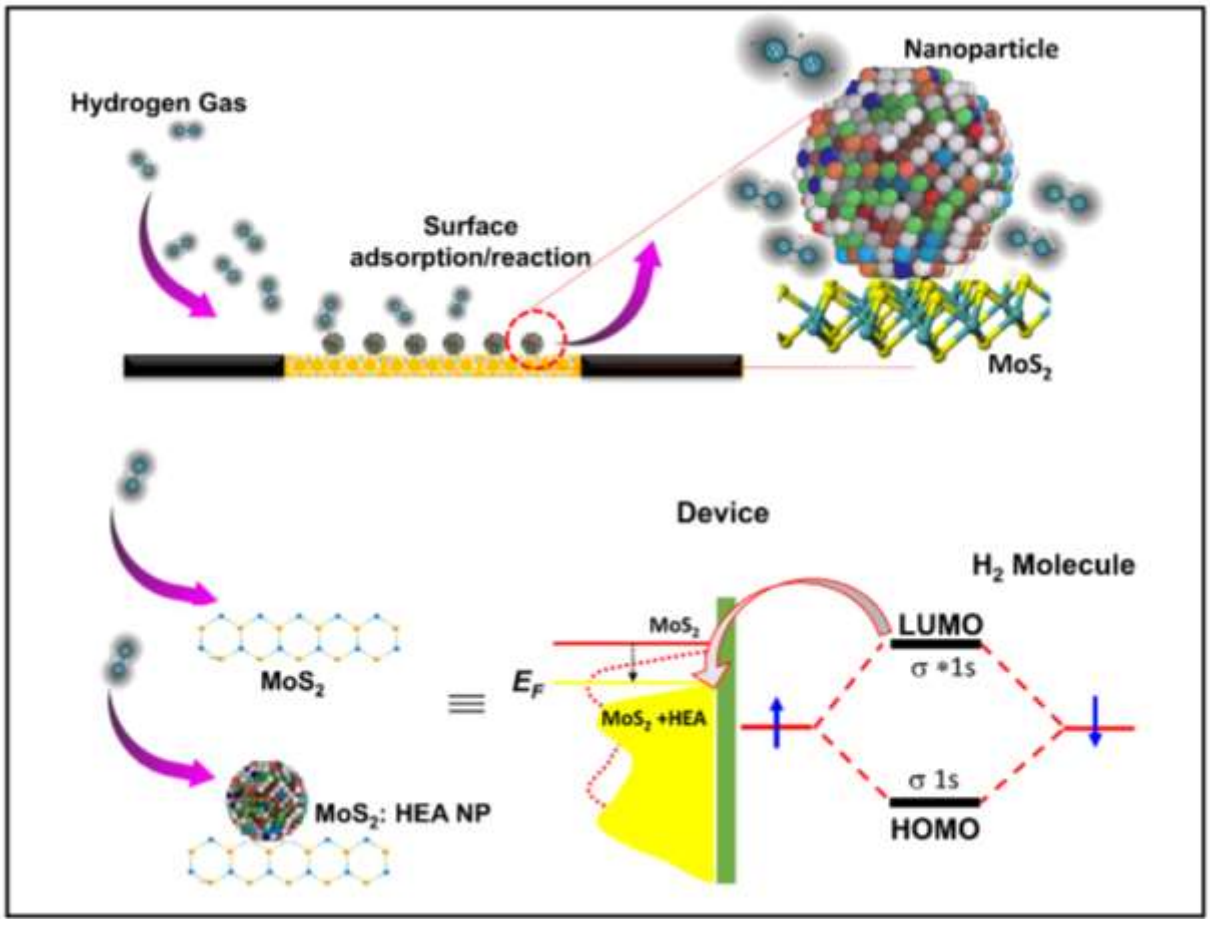

Fig. 5 Schematic of hydrogen adsorption on MoS_2 and HEA: MoS_2 and electron transfer from H_2 molecules to HEA: MoS_2

Conclusion

Through novel experiments and DFT simulations, we have highlighted the underlying mechanism behind the performance gain in the sensitivity of the signal from 7% to 47% to sense hydrogen through simple functionalization of the 2D MoS_2 sheets with the alloyed HEA nanoparticles consisting of non-noble metals. Our approach involved a material system relying on functionalisation (decoration) of the Ti-Zr-V-Nb-Hf High entropy alloy (HEA) nanoparticles on top of the 2D MoS2 sheets and it showed a unique behavior to dissociate and adsorb hydrogen molecules by electronic charge redistribution at the interface. We performed fabrication, testing and supporting numerical studies to develop a low-cost sensor for ambient temperature detection of hydrogen and a few other gases. The Raman shifts results provide direct evidence of charge redistribution, while our DFT calculations indicate more favorable enhanced adsorption of H_2 molecules. These findings highlight the potential of using HEA nanoparticles as a promising material in gas sensing applications at room temperature, and the ability to enhance the performance of MoS_2-based sensors as alternatives to expensive Pd metal NPs.

Author contributions

B Mondal: investigation, experimental work, and wrote the original draft. X Zhang: DFT calculations. S Kumar: investigation, experimental work, and wrote the original draft. F Long: DFT calculations investigation. N K Katiyar: investigation, experimental work, and wrote the original draft. M Kumar: defined the problem, Methodology, Supervision, and editing. S Goel: defined the problem, Methodology, Supervision, and editing. K Biswas: defined the problem, Methodology, Supervision, and editing.

Conflict of Interest

There are no conflicts to declare.

Acknowledgments

The author would like to thank the Department of Science and Technology (DST) India for providing funds to carry out this project part of the M.Tech Thesis. SG would like to acknowledge the financial support provided by the UKRI via Grants No. EP/S036180/1 and EP/T024607/1, Hubert Curien Partnership Programme from the British Council and the International exchange Cost Share award by the Royal Society (IEC\NSFC\223536). Additionally, we are grateful to be granted the access of various HPC resources including ARCHIE-West (Research Computing for the West Scotland), the Isambard Bristol, UK supercomputing service as well as Kittrick (LSBU, UK), Magus2 (Shiv Nadar University, India) and Param Ishan (IIT Guwahati, India).

References

1. S. van Renssen, Nat. Clim. Change., 2020, 10, 799-801.
2. M. Molnarne and V. Schroeder, Process Saf Environ Pr, 2019, 130, 1-5.
3. H.-S. Lee, J. Kim, H. Moon and W. Lee, Adv. Mater., 2021, 33, 2005929.
4. F. Favier, E. C. Walter, M. P. Zach, T. Benter and R. M. Penner, Science, 2001, 293, 2227-2231.
5. F. Yang, D. K. Taggart and R. M. Penner, Small, 2010, 6, 1422-1429.
6. X. Li, Y. Liu, J. C. Hemminger and R. M. Penner, ACS Nano, 2015, 9, 3215-3225.
7. I. Darmadi, S. Z. Khairunnisa, D. Tomeček and C. Langhammer, ACS Appl. Nano Mater, 2021, 4, 8716-8722.
8. K. Namba, S. Ogura, S. Ohno, W. Di, K. Kato, M. Wilde, I. Pletikosić, P. Pervan, M. Milun and K. Fukutani, PNAS, 2018, 115, 7896-7900.
9. E. P. George, D. Raabe and R. O. Ritchie, Nat. Rev. Mater., 2019, 4, 515-534.
10. K. M. B. Urs, N. K. Katiyar, R. Kumar, K. Biswas, A. K. Singh, C. S. Tiwary and V. Kamble, Nanoscale, 2020, 12, 11830-11841.
11. N. K. Katiyar, K. Biswas and C. S. Tiwary, Int. Mater. Rev., 2020, 66, 493-532.
12. N. K. Katiyar, K. Biswas, C. S. Tiwary, L. D. Machado and R. K. Gupta, Langmuir, 2019, 35, 2668-2673.
13. N. Kumar and K. Biswas, Rev. Sci. Instrum., 2015, 86, 083903-083908.
14. N. K. Katiyar, S. Dhakar, A. Parui, P. Gakhad, A. K. Singh, K. Biswas, C. S. Tiwary and S. Sharma, ACS Catal., 2021, 11, 14000-14007.
15. S. Dhakar, A. Sharma, N. K. Katiyar, A. Parui, R. Das, A. K. Singh, C. S. Tiwary, S. Sharma and K. Biswas, Mater. Today Eng., 2023, 101386.

16. J. P. Perdew and Y. Wang, Phys. Rev. B, 1992, 45, 13244-13249.
17. G. Kresse and J. Furthmüller, Comput. Mater. Sci, 1996, 6, 15-50.
18. J. P. Perdew, K. Burke and M. Ernzerhof, Phys. Rev. Lett., 1996, 77, 3865-3868.
19. K. L. Kelly, E. Coronado, L. L. Zhao and G. C. Schatz, J. Phys. Chem. B, 2003, 107, 668-677.
20. X. Zheng, W. Chen, G. Wang, Y. Yu, S. Qin, J. Fang, F. Wang and X.-A. Zhang, AIP Advances, 2015, 5, 057133.
21. Y. Zhai, H. Yang, S. Zhang, J. Li, K. Shi and F. Jin, J. Mater. Chem. C, 2021, 9, 6823-6833.
22. S. E. Panasci, E. Schilirò, G. Greco, M. Cannas, F. M. Gelardi, S. Agnello, F. Roccaforte and F. Giannazzo, ACS Appl. Mater. Interfaces, 2021, 13, 31248-31259.
23. S. McDonnell, R. Addou, C. Buie, R. M. Wallace and C. L. Hinkle, ACS Nano, 2014, 8, 2880-2888.
24. K. A. Rickert, A. B. Ellis, J. K. Kim, J. L. Lee, F. J. Himpsel, F. Dwikusuma and T. F. Kuech, *J. Appl. Phys*, 2002, **92**, 6671–6678.
25. E. Hökelek and G. Y. Robinson, *J. Appl. Phys.*, 1983, **54**, 5199–5205.
26. A. J. Chiquito, C. A. Amorim, O. M. Berengue, L. S. Araujo, E. P. Bernardo and E. R. Leite, *J. Phys.: Condens. Matter,*2012*, **24,** 225303.*
27. B. Liu, L. Chen, G. Liu, A. N. Abbas, M. Fathi and C. Zhou, ACS Nano, 2014, 8, 5304-5314.
28. H. Yang, Y. Liu, C. Gao, L. Meng, Y. Liu, X. Tang and H. Ye, *J. Phys. Chem. C*, 2019, **123**, 30949–30957.
29. S. Kumar, R. Chaurasiya, M. A. Khan, G. Meng, J.-S. Chen and M. Kumar, *J. Phys.: Condens. Matter, 2022,* **35,** 064001
30. R. Aso, H. Hojo, Y. Takahashi, T. Akashi, Y. Midoh, F. Ichihashi, H. Nakajima, T. Tamaoka, K. Yubuta, H. Nakanishi, H. Einaga, T. Tanigaki, H. Shinada and Y. Murakami, Science, 2022, 378, 202-206.
31. R. C. Lochan and M. Head-Gordon, Phys. Chem. Chem. Phys., 2006, 8, 1357-1370.
32. O. V. Yazyev and A. Kis, Mater. Today, 2015, 18, 20-30.